AJNR

Bayesian Estimation of CBF Measured by DSC-MRI in Patients with Moyamoya Disease: Comparison with ^{15}O-Gas PET and Singular Value Decomposition

S. Hara, Y. Tanaka, S. Hayashi, M. Inaji, T. Maehara, M. Hori, S. Aoki, K. Ishii and T. Nariai

Bayesian Estimation of CBF Measured by DSC-MRI in Patients with Moyamoya Disease: Comparison with ^{15}O-Gas PET and Singular Value Decomposition

S. Hara, Y. Tanaka, S. Hayashi, M. Inaji, T. Maehara, M. Hori, S. Aoki, K. Ishii, and T. Nariai

ABSTRACT

BACKGROUND AND PURPOSE: CBF analysis of DSC perfusion using the singular value decomposition algorithm is not accurate in patients with Moyamoya disease. This study compared the Bayesian estimation of CBF against the criterion standard PET and singular value decomposition methods in patients with Moyamoya disease.

MATERIALS AND METHODS: Nineteen patients with Moyamoya disease (10 women; 22–52 years of age) were evaluated with both DSC and ^{15}O-gas PET within 60 days. DSC-CBF maps were created using Bayesian analysis and 3 singular value decomposition analyses (standard singular value decomposition, a block-circulant deconvolution method with a fixed noise cutoff, and a block-circulant deconvolution method that adopts an occillating noise cutoff for each voxel according to the strength of noise). Qualitative and quantitative analyses of the Bayesian-CBF and singular value decomposition–CBF methods were performed against ^{15}O-gas PET and compared with each other.

RESULTS: In qualitative assessments of DSC-CBF maps, Bayesian-CBF maps showed better visualization of decreased CBF on PET (sensitivity = 62.5%, specificity = 100%, positive predictive value = 100%, negative predictive value = 78.6%) than a block-circulant deconvolution method with a fixed noise cutoff and a block-circulant deconvolution method that adopts an oscillating noise cutoff for each voxel according to the strength of noise ($P < .03$ for all except for specificity). Quantitative analysis of CBF showed that the correlation between Bayesian-CBF and PET-CBF values ($\rho = 0.46$, $P < .001$) was similar among the 3 singular value decomposition methods, and Bayesian analysis overestimated true CBF (mean difference, 47.28 mL/min/100 g). However, the correlation between CBF values normalized to the cerebellum was better in Bayesian analysis ($\rho = 0.56$, $P < .001$) than in the 3 singular value decomposition methods ($P < .02$).

CONCLUSIONS: Compared with previously reported singular value decomposition algorithms, Bayesian analysis of DSC perfusion enabled better qualitative and quantitative assessments of CBF in patients with Moyamoya disease.

ABBREVIATIONS: CBF% = CBF values normalized to the cerebellum; cSVD = block-circulant deconvolution method with a fixed noise cutoff; oSVD = block-circulant deconvolution method that adopts an oscillating noise cutoff for each voxel according to the strength of noise; SVD = singular value decomposition; sSVD = standard SVD

DSC-PWI is an MR imaging–based perfusion measurement that relies on the measurement of T2* decrease during the first pass of an exogenous endovascular tracer through the capillary bed.[1,2] It obtains multiple hemodynamic parameters, including CBV, MTT, and CBF, by a single scan within a clinically feasible scanning duration.[3] Because of the better clinical availability and lower invasiveness of MR imaging compared with the criterion standard PET method, DSC is widely used for the assessment of cerebrovascular diseases.[3] There are

many variations in the postprocessing of DSC, such as first-pass and singular value decomposition (SVD).[1,2] Although time-based perfusion parameters, such as the time of maximum concentration and MTT, are clinically useful in acute stroke[4] or chronic cerebrovascular disease such as Moyamoya disease,[5] the correlation between the CBF values obtained by SVD methods and by the criterion standard PET method is not sufficient, especially in patients with Moyamoya disease.[3,5-10]

Recently, Bayesian probabilistic analysis, which uses the Bayes theorem for parameter estimation, has emerged as a novel method to analyze DSC.[11] Bayesian analysis of DSC is more robust to noise and errors such as tracer delay and offers more accurate estimation of hemodynamic parameters such as CBF and MTT than SVD methods.[12] To date, the clinical feasibility of Bayesian perfusion analysis has been widely reported in acute stroke,[13,14] reduced contrast-dose protocols,[15] and the separation of tissue types of glioma.[16] It is possible that DSC-CBF obtained by Bayesian analysis reflects true CBF much better than SVD methods. However, to the best of our knowledge, no study has investigated the CBF accuracy of Bayesian analysis using PET as the criterion standard.

The purpose of this study was to investigate the accuracy of DSC-CBF obtained from Bayesian analysis in patients with Moyamoya disease—that is, chronic occlusive cerebrovascular disease with strong transit delay and increased CBV—compared with the criterion standard ^{15}O-gas PET and the SVD analysis of DSC.

MATERIALS AND METHODS

Patient Selection Protocol

This retrospective study was approved by the ethics committee of Tokyo Medical and Dental University (M2000-1331). We reviewed medical records from January 2014 to October 2015 and found 19 patients (10 women, 22–52 years of age) who were diagnosed with Moyamoya disease according to the diagnostic guidelines[17] and were evaluated with DSC and ^{15}O-gas PET within an interval of <60 days. Of 19 patients, 13 patients had an ischemic presentation (TIA and/or infarction) and 6 patients had a hemorrhagic event. The infarction and hemorrhage occurred >3 weeks before the imaging studies. Three patients received surgical treatment >200 days before the imaging period. The full details of the patient characteristics are described in On-line Table 1. All patients except 1 were evaluated with DSC before ^{15}O-gas PET, and no new lesions or symptoms occurred between the evaluations. None of the patients with TIA experienced TIA during or immediately before the DSC and PET studies.

DSC Acquisition and CBF Analysis

We used a 3T MR imaging scanner (Signa HDxt; GE Healthcare, Milwaukee, Wisconsin) with an 8-channel head coil and acquired gradient recalled-echo single-shot multislice EPI with a TR of 1000 ms, a TE of 40 ms, an FOV of 22 cm, a voxel size of 1.78 × 1.78 mm, and a matrix size of 128 × 128. A series of seven 5-mm-thick slices separated by 7.5-mm gaps was acquired after a bolus injection of gadodiamide (0.2 mmol/kg body weight, Omniscan 32%; GE Healthcare, Piscataway, New Jersey) via an antecubital vein using a power injector (Sonic Shot GX; Nemoto Kyorindo, Tokyo, Japan) at a rate of 3 mL/s, followed by a 15-mL saline flush.[5] The acquisition time was 3 minutes.

Acquired data were transferred to a personal computer with commercially available software, Olea Sphere, Version 3.0 (Olea Medical Solutions, La Ciotat, France) implemented with 4 DSC analyses: standard SVD (sSVD);[1] a block-circulant deconvolution method with a fixed noise cutoff (cSVD);[18] a block-circulant deconvolution method with an oscillating noise cutoff for each voxel according to the strength of noise (oSVD);[9,18] and Bayesian probabilistic analysis (Bayesian).[11,19] The motion correction (rigid coregistration) was automatically performed to fit all acquired images to a single reference image selected by the software algorithm. The arterial input function was automatically selected using a cluster analysis algorithm that reduces bias due to delay and dispersion,[20] and the same arterial input function was applied to all 4 analytic methods in each patient.

PET Data Acquisition

The PET data were acquired using a Discovery 710 PET/CT scanner (GE Healthcare).[21] The 3.5-minute acquisition of the scans was initiated simultaneously with a 1.5-minute inhalation of $C^{15}O_2$ (2000 MBq/min) and $C^{15}O$ (2000 MBq/min) using a neck shield.[22] The amount of radioactivity in the arterial whole blood was manually collected at 0, 2, and 4 minutes, and images of inhaled $C^{15}O_2$ were also acquired.[23] The images were reconstructed under the following conditions: a 3D-ordered-subset expectation-maximization algorithm, 128 × 128 matrix, 47 slices, 2.0 mm/pixel, 3.27-mm/section, 4 iterations, 16 subsets, and a Gaussian filter of 3.0 mm. The amount of radioactivity in the arterial blood was used to create CBF and CBV images using the PET autoradiographic method with Xeleris software (GE Healthcare).[25]

Visual Assessment of CBF Maps

Three neurosurgeons who specialized in cerebral perfusion (S. Hara, Y.T., and T.N., with 10, 23, and 34 years of clinical experience, respectively) assessed the presence of decreased CBF in each hemisphere of each absolute CBF map. The assessments were performed on separate occasions. Each surgeon was blinded to the patient information, except for the location of brain lesions (infarctions and hemorrhages) that should not be included in the visual assessments and the type of CBF analytic method, and each was without access to the conclusions of the other surgeons. During the assessment, each map was shown in the visually appropriate color scales to show similar contrasts; in the software we used (Dr. View R2.5; Infocom, Tokyo, Japan), the upper and lower thresholds of the color ranges were set to exclude the top 10% and the bottom 30% of the voxels of the histogram of each map. If necessary, the upper threshold was sometimes changed to produce similar contrasts. The median answer of the 3 evaluators was recorded as a consensus.

Calculation of Regional Values

PET and MR images were spatially coregistered using the image-registration function of Dr. View R2.5. Because our DSC is not 3D data, we reconstructed the PET-CBF and PET-CBV maps into 7 slices matched to the DSC maps using the raw DSC image of each patient as a reference. The ROIs were manually drawn on the raw DSC images over 10 cortical areas (bilateral frontal, parietal, rolandic, temporal, and occipital lobes) and the cerebellum,[5,26,27] as shown in On-line Fig 1, by a single neurosurgeon (S. Hara) who was blinded to the clinical information of the patients. The brain lesions visible on the raw DSC images (infarctions and hemorrhages) were omitted from the ROIs. To evaluate
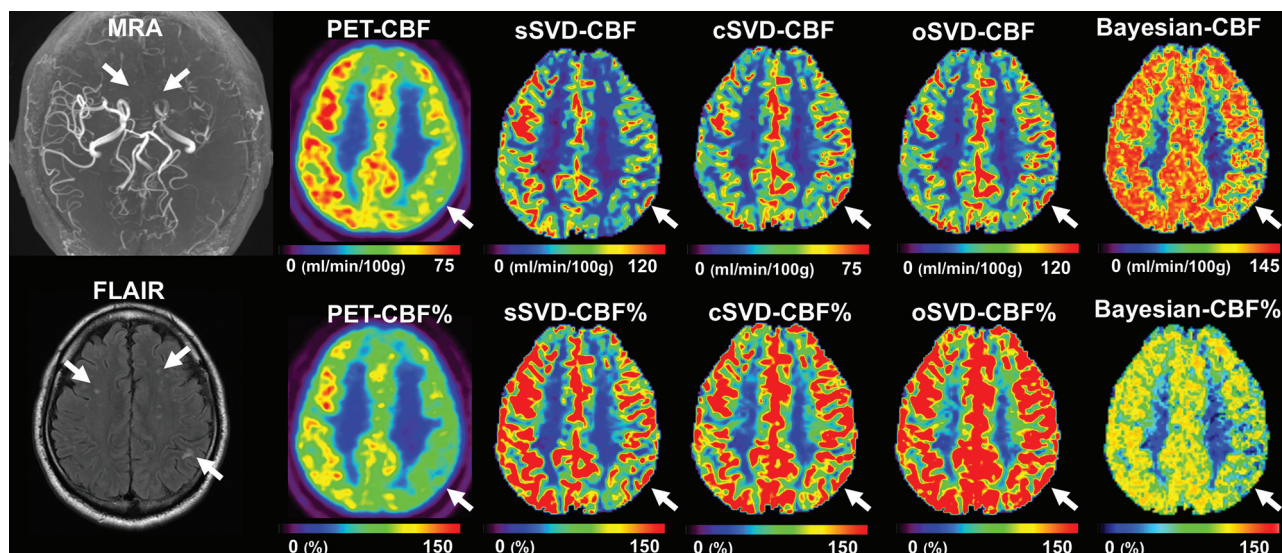
FIG 1. A representative case. A 48-year-old man was incidentally diagnosed with Moyamoya disease by nonspecific symptoms. MRA reveals occlusion of the terminal portion of the left ICA (*arrows*), bilateral anterior cerebral arteries, and the left MCA. FLAIR shows bilateral white matter hyperintensities. CBF maps obtained by PET, sSVD and Bayesian analysis shows clearly reduced CBF on the left sides (*arrows*). However, the CBF maps obtained by cSVD and oSVD do not show the laterality of the CBF that is evident on PET (*arrows*). The CBF% map of Bayesian analysis shows values close to the CBF% of PET. Please note that the color scale used in the raw CBF maps was the same as that used during the visual assessments and that the color scales of the CBF% maps were unified.

intrareader variability, ROIs were drawn twice for 40 randomly selected regions.

Statistical Analysis

Qualitative Analysis. We counted the number of hemispheres that were considered to exhibit a decrease in CBF on PET-CBF maps and the number of hemispheres in which the DSC-derived CBF maps were correctly correlated with the PET maps. Then, we calculated the sensitivity, specificity, positive predictive value, and negative predictive value of the visual assessment of CBF maps acquired by 4 DSC analytic methods using the decreased CBF on PET maps as the true-positive finding. The sensitivity and specificity were compared using the McNemar test, and weighted generalized score statistics were used to compare positive and negative predictive values.

Quantitative Analysis. The interclass correlation coefficient was calculated from 40 randomly selected areas where ROIs were drawn twice. The distribution of the CBF values of each technique was evaluated with the Shapiro-Wilk test for normality.

The correlation coefficients between the regional CBF values of 10 cortical areas (not including the cerebellum) in all patients obtained by the 4 analyses and PET were calculated and tested for significance using the Fisher *Z* transformation. By means of the Bland-Altman analysis, the average, 95% confidence intervals, and limits of agreement (average $\pm$ 1.96 $\times$ SDs) of the difference between DSC-CBF and PET-CBF and the correlation coefficients between the average and the difference between DSC-CBF and PET-CBF values were calculated. Because the software we used reported the DSC-CBF values in "arbitrary units (milliliters/minute/100 g)," the relationship among the CBF values normalized to the cerebellum (CBF%) was evaluated in addition to the relationship among the raw values. We also compared the correlation

between the DSC-CBF and PET-CBF values in hemispheres with visually decreased CBF and in hemispheres with visually normal CBF determined by the qualitative analysis described above. The relationship between PET-CBV and DSC-CBV in each method was also evaluated.

All statistical analyses were performed using R, Version 3.2.2 (https://cran.r-project.org), and $P < .05$ was regarded as significant.

RESULTS

Qualitative Analysis

A representative case is shown in Fig 1. Of 38 hemispheres of 19 patients, 16 (42%) hemispheres were considered to have decreased CBF. The number of hemispheres that DSC-derived CBF maps correctly correlated with PET (ie, true-positive/true-negative) was 10/19 in sSVD, 3/19 in cSVD, 5/20 in oSVD, and 10/22 in Bayesian analysis. Overall, visual assessments of Bayesian-CBF maps offered higher sensitivity, specificity, positive predictive values, and negative predictive values than cSVD and oSVD, but these values did not significantly differ from those obtained by sSVD (Table and On-line Table 2).

Quantitative Analysis

The interclass correlation coefficients of each technique were 0.95–0.99. Because many CBF values were not normally distributed ($P = <.0001$–.35), we used Spearman correlation coefficients (ρ) to evaluate the CBF correlations between each technique.

The correlation between the absolute cerebral CBF values of PET and those of DSC analyses were moderate (Fig 2). The correlation strength of the Bayesian analysis was significantly better than that of sSVD but not better than that of oSVD and cSVD

(On-line Table 3). Bland-Altman analysis revealed that the Bayesian method overestimates CBF compared with PET, with strong constant bias and small proportional bias.

Among the correlation analyses of CBF% values, Bayesian-CBF% showed the best correlation with PET-CBF% (Fig 3), significantly better than those of the 3 SVD methods (On-line Table 3). The 3 SVD methods overestimated the CBF% values compared with PET, with significant proportional bias that was not observed in the Bayesian method.

When comparing the relationship between DSC-CBF and PET-CBF values in decreased CBF hemispheres and in normal CBF hemispheres, the difference between DSC-CBF% and PET-CBF% was larger and the proportional bias stronger in decreased CBF hemispheres than in normal CBF hemispheres in the sSVD, cSVD, and oSVD methods (On-line Table 4). In contrast, in the Bayesian method, the difference between DSC-CBF% and PET-CBF% was not higher in decreased CBF hemispheres than in normal CBF hemispheres.

The correlation between PET-CBV and DSC-CBV in each method did not differ significantly (On-line Fig 2 and On-line Table 5).

DISCUSSION

We demonstrated that Bayesian analysis depicted true CBF qualitatively and quantitatively compared with SVD methods in patients with Moyamoya disease. Although a good correlation between SVD-measured CBF and PET-CBF has been reported in analyses of pig stroke and a small number of healthy volunteers,[9,28-30] the SVD-CBF values did not correlate well with true CBF in patients with cerebrovascular diseases, especially in patients with Moyamoya disease.[5,26] The effect of global perfusion delay on arterial input function values and increased tissue signals caused by increased CBV are thought to negatively affect the accuracy of DSC-CBF values in these patients. In the Bayesian analysis of DSC, instead of simply fitting the observed tissue signal to the deconvolution formula, as in SVD analysis, the observed tissue signal was reconvoluted to create the CBF map, considering the accurate movement of the residue fraction of the injected tracer and the probability distribution of CBF values. This algorithm enables better assumptions for CBF, unaffected by tracer delay effects and increased noise signals from increased CBV, which are both prominent in patients with Moyamoya disease.[31]

Interestingly, the oldest SVD method (sSVD) was superior in qualitative analysis to the newer SVD methods (cSVD and oSVD) in terms of sensitivity to decreased regional CBF. The linear deconvolution used in sSVD is sensitive to the tracer-arrival delay effect that leads to the underestimation of CBF in regions with perfusion delay. The circular deconvolution used in cSVD and oSVD is proposed to eliminate the effect of tracer-arrival delay; cSVD
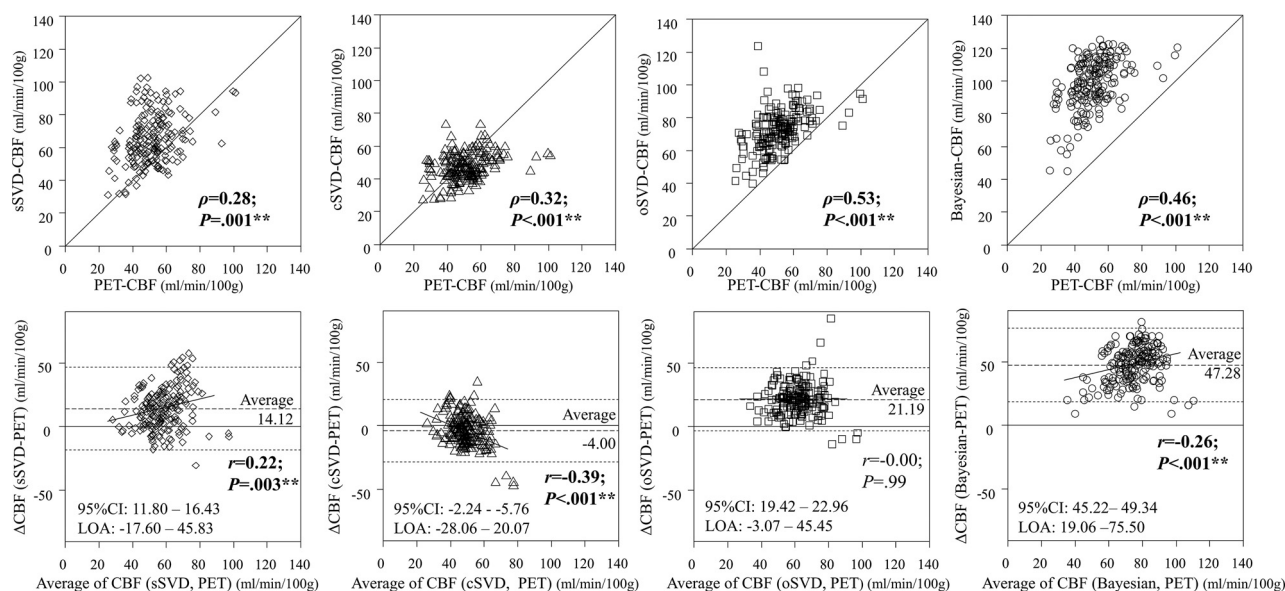
Sensitivity, specificity, positive predictive value, and negative predictive value of the visual assessment of the 4 DSC-CBF maps[a]

(%)	sSVD	cSVD	oSVD	Bayesian
Sensitivity	62.5 (35.4–84.8)[b]	18.8 (4.0–45.6)	31.3 (11.0–58.7)[c]	62.5 (35.4–84.8)[b]
Specificity	86.4 (65.1–97.1)	86.4 (65.1–97.1)	90.9 (70.8–98.9)	100 (78.1–100)
Positive predictive value	76.9 (46.2–95.0)	50.0 (11.8–88.2)	71.4 (29.0–96.3)	100 (58.7–100)[c]
Negative predictive value	76.0 (54.9–90.6)	59.4 (40.6–76.3)	64.5 (45.4–80.8)	78.6 (59.0–91.7)[b]

[a] Data are averages and 95% CI.
[b] $P < .05$ compared with cSVD and oSVD.
[c] $P < .05$ compared with cSVD.

FIG 2. The Bland-Altmann analysis between the regional raw CBF values of PET and each of the 4 DSC analyses. All methods showed moderate correlation between DSC and PET, and there was no significant difference between Bayesian analysis and the other SVD methods except for sSVD (versus cSVD, $P = .11$; versus oSVD, $P = .37$; versus sSVD, $P = .04$). sSVD overestimates PET-CBF with a small proportional bias; cSVD underestimates PET-CBF with moderate negative proportional bias; oSVD overestimates PET-CBF without proportional bias; and Bayesian-CBF strongly overestimates PET-CBF with a small proportional bias. LOA, limits of agreement defined as average $\pm$ 1.96 $\times$ SD. *$P < .05$ and **$P < .005$.
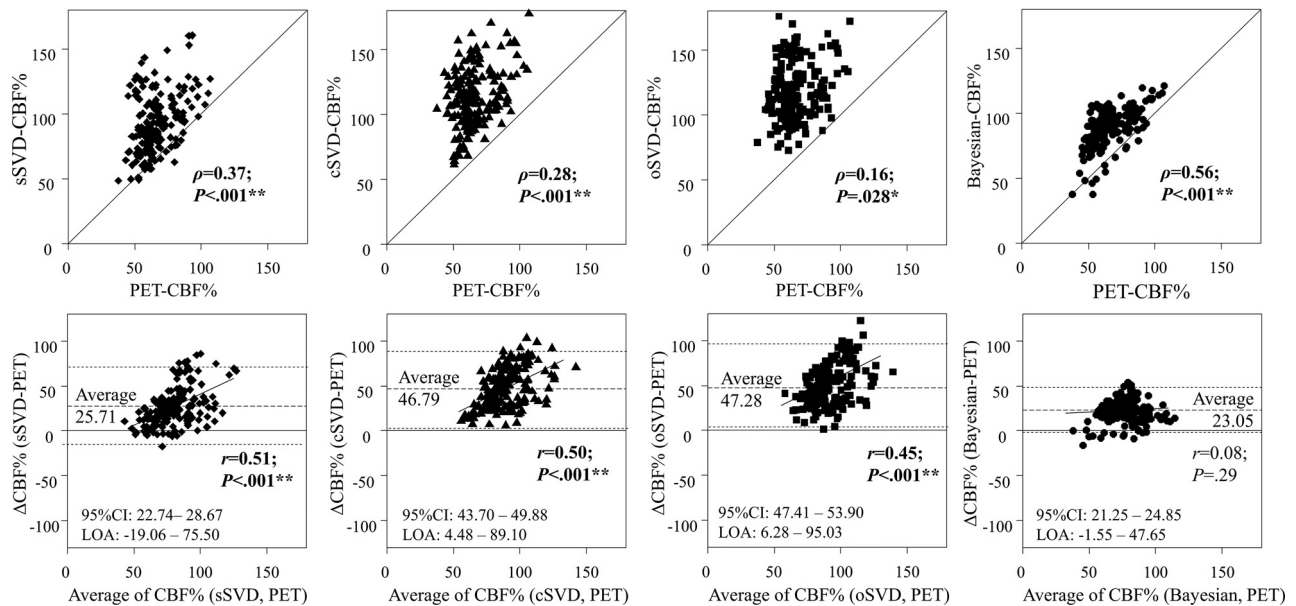
FIG 3. The Bland-Altmann analysis between the regional CBF values normalized to cerebellum (CBF%) of PET and the 4 DSC analyses. The correlation of the Bayesian analysis was significantly better than those of the 3 SVD methods (versus sSVD, $P = .02$; versus cSVD, $P < .001$; versus oSVD, $P < .001$). The limit of agreement (LOA, defined as average ±1.96 x SD) of the Bayesian method was also smaller than those of the 3 SVD methods. *$P < .05$ and **$P < .005$.

uses a global fixed threshold to eliminate noise, while the oSVD uses a different threshold in every voxel according to the strength of noise and is less sensitive to the effect of CBV than cSVD.[18] Therefore, in theory, oSVD-CBF should be the best method to depict CBF in patients with Moyamoya disease who exhibit increased CBV and prominent perfusion delay,[31,32] which was the opposite of what was actually observed. We also found that when SVD methods were used, the difference between DSC-CBF% and PET-CBF% was larger in hemispheres with decreased CBF than in normal CBF hemispheres, as indicated by the significant proportional bias. We speculated that the strongly increased CBV in our patients with Moyamoya overwhelmed the correction ability of the block-circulant methods and led to the improperly increased CBF signal in the affected regions. On the other hand, tracer arrival delay, which is strong in Moyamoya disease, might overwhelm the effect of increased signals resulting from increased CBV and lead to the proper depiction of decreased CBF in the sSVD method. It may be better to choose sSVD instead of cSVD or oSVD to qualitatively depict the decrease in CBF in patients with Moyamoya disease if Bayesian analysis is unavailable.

We found that Bayesian analysis was superior for the quantitative evaluation of CBF values normalized to the cerebellum but not the raw CBF values; all methods except oSVD overestimated the CBF values, and the overestimation was particularly prominent in the Bayesian method. Considering the completely different mechanisms of DSC using an intravascular tracer and PET using a diffusible tracer, it is not surprising that the raw CBF values of PET and DSC do not correlate well. The correlation of CBF values in the cerebellum, where CBF is unaffected and is used as a control in patients with Moyamoya disease, is also not perfect in any method (On-line Fig 3). In addition to the different

tracer mechanisms, we speculated that the Bayesian analytic method essentially overestimates CBF values, possibly due to the higher values of the CBF distribution used in this software compared with the CBF distribution of ^{15}O-gas PET. However, the qualitative assessments using CBF values in reference to the cerebellum were better in Bayesian analysis than in the SVD methods. Additionally, the difference between the Bayesian-CBF% and PET-CBF% values was smaller than the differences obtained by the SVD methods, regardless of the presence of decreased CBF, suggesting that the Bayesian analytic method is more robust than the SVD methods to the errors resulting from increased CBV and transit time in patients with Moyamoya disease. In addition to the better CBF depiction ability we showed, the MTT values from the Bayesian method are shown to be superior to those from SVD methods,[19] and the correlation between DSC-CBV and PET-CBV was not different among the DSC methods. Considering that MTT values are biomarkers of clinical presentation,[32] increased oxygen extraction fraction,[5] and surgical outcome[33,34] in patients with Moyamoya disease, Bayesian analysis would be a better choice than SVD methods to analyze DSC in these patients.

The limitations of our study include the small sample size and the relatively long DSC-PET intervals, which were inevitable due to the limited availability of PET examinations. We did not perform first-pass method analysis, which was not implemented in our software. Considering the software-dependent nature of DSC analysis,[12] different analysis software must produce different results; however, to the best of our knowledge, the software we used is the only commercially available software that implements Bayesian analysis. Although several limitations exist, our results suggest that Bayesian analysis might be the current best method to analyze DSC-PWI in patients with Moyamoya disease.

CONCLUSIONS

Bayesian analysis of DSC perfusion enabled better qualitative and quantitative assessments of CBF in patients with Moyamoya disease than previously reported SVD algorithms.

ACKNOWLEDGMENTS

We thank Professor Kohsuke Kudo for suggestions regarding the interpretation of the results and Dr Masako Akiyama for statistical guidance.

REFERENCES

1. Ostergaard L, Weisskoff RM, Chesler DA, et al. **High-resolution measurement of cerebral blood flow using intravascular tracer bolus passages, part I: mathematical approach and statistical analysis.** *Magn Reson Med* 1996;36:715–75 CrossRef Medline

2. Ostergaard LW, Chesler DA, Gyldensted C, et al. **High resolution measurement of cerebral blood flow using intravascular tracer bolus passages, part II: experimental comparison and preliminary results.** *Magn Reson Med* 1996;36:726–36 CrossRef Medline

3. Wintermark M, Sesay M, Barbier E, et al. **Comparative overview of brain perfusion imaging techniques.** *Stroke* 2005;36:e83–99 CrossRef Medline

4. Lansberg MG, Lee J, Christensen S, et al. **RAPID automated patient selection for reperfusion therapy: a pooled analysis of the Echoplanar Imaging Thrombolytic Evaluation Trial (EPITHET) and the Diffusion and Perfusion Imaging Evaluation for Understanding Stroke Evolution (DEFUSE) Study.** *Stroke* 2011;42:1608–14 CrossRef Medline

5. Tanaka Y, Nariai T, Nagaoka T, et al. **Quantitative evaluation of cerebral hemodynamics in patients with Moyamoya disease by dynamic susceptibility contrast magnetic resonance imaging: comparison with positron emission tomography.** *J Cereb Blood Flow Metab* 2006;26:291–300 CrossRef Medline

6. Ibaraki M, Shimosegawa E, Toyoshima H, et al. **Effect of regional tracer delay on CBF in healthy subjects measured with dynamic susceptibility contrast-enhanced MRI: comparison with 15O-PET.** *Magn Reson Med Sci* 2005;4:27–34 CrossRef Medline

7. Lin W, Celik A, Derdeyn C, et al. **Quantitative measurements of cerebral blood flow in patients with unilateral carotid artery occlusion: a PET and MR study.** *J Magn Reson Imaging* 2001;14:659–67 CrossRef Medline

8. Mukherjee P, Kang HC, Videen TO, et al. **Measurement of cerebral blood flow in chronic carotid occlusive disease: comparison of dynamic susceptibility contrast perfusion MR imaging with positron emission tomography.** *AJNR Am J Neuroradiol* 2003;24:862–71 Medline

9. Ostergaard L, Johannsen P, Host-Poulsen P, et al. **Cerebral blood flow measurements by magnetic resonance imaging bolus tracking: comparison with [(15)O]H2O positron emission tomography in humans.** *J Cereb Blood Flow Metab* 1998;18:935–40 CrossRef Medline

10. Vakil P, Lee JJ, Mouannes-Srour JJ, et al. **Cerebrovascular occlusive disease: quantitative cerebral blood flow using dynamic susceptibility contrast MR imaging correlates with quantitative H2[15O] PET.** *Radiology* 2013;266:879–86 CrossRef Medline

11. Boutelier T, Kudo K, Pautot F, et al. **Bayesian hemodynamic parameter estimation by bolus tracking perfusion weighted imaging.** *IEEE Trans Med Imaging* 2012;31:1381–95 CrossRef Medline

12. Kudo K, Christensen S, Sasaki M, et al. **Accuracy and reliability assessment of CT and MR perfusion analysis software using a digital phantom.** *Radiology* 2013;267:201–11 CrossRef Medline

13. Kudo K, Boutelier T, Pautot F, et al. **Bayesian analysis of perfusion-weighted imaging to predict infarct volume: comparison with singular value decomposition.** *Magn Reson Med Sci* 2014;13:45–50 CrossRef Medline

14. Nicoli F, Scalzo F, Saver JL, et al. **The combination of baseline magnetic resonance perfusion-weighted imaging-derived tissue volume with severely prolonged arterial-tissue delay and diffusion-weighted imaging lesion volume is predictive of MCA-M1 recanalization in patients treated with endovascular thrombectomy.** *Neuroradiology* 2014;56:117–27 CrossRef Medline

15. Nael K, Mossadeghi B, Boutelier T, et al. **Bayesian estimation of cerebral perfusion using reduced-contrast-dose dynamic susceptibility contrast perfusion at 3T.** *AJNR Am J Neuroradiol* 2015;36:710–18 CrossRef Medline

16. Hansen MB, Tietze A, Kalpathy-Cramer J, et al. **Reliable estimation of microvascular flow patterns in patients with disrupted blood-brain barrier using dynamic susceptibility contrast MRI.** *J Magn Reson Imaging* 2017;46:537–49 CrossRef Medline

17. Research Committee on the Pathology and Treatment of Spontaneous Occlusion of the Circle of Willis; Health Labour Sciences Research Grant for Research on Measures for Infractable Diseases. **Guidelines for diagnosis and treatment of Moyamoya disease (spontaneous occlusion of the circle of Willis).** *Neurol Med Chir (Tokyo)* 2012;52:245–66 CrossRef Medline

18. Wu O, Ostergaard L, Weisskoff RM, et al. **Tracer arrival timing-insensitive technique for estimating flow in MR perfusion-weighted imaging using singular value decomposition with a block-circulant deconvolution matrix.** *Magn Reson Med* 2003;50:164–74 CrossRef Medline

19. Sasaki M, Kudo K, Boutelier T, et al. **Assessment of the accuracy of a Bayesian estimation algorithm for perfusion CT by using a digital phantom.** *Neuroradiology* 2013;55:1197–1203 CrossRef Medline

20. Mouridsen K, Christensen S, Gyldensted L, et al. **Automatic selection of arterial input function using cluster analysis.** *Magn Reson Med* 2006;55:524–31 CrossRef Medline

21. Bettinardi V, Presotto L, Rapisarda E, et al. **Physical performance of the new hybrid PETCT Discovery-690.** *Med Phys* 2011;38:5394–5411 CrossRef Medline

22. Shidahara M, Watabe H, Kim KM, et al. **Optimal scan time of oxygen-15-labeled gas inhalation autoradiographic method for measurement of cerebral oxygen extraction fraction and cerebral oxygen metabolic rate.** *Ann Nucl Med* 2008;22:667–75 CrossRef Medline

23. Kudomi N, Choi E, Yamamoto S, et al. **Development of a GSO detector assembly for a continuous blood sampling system.** *IEEE Trans Nucl Sci* 2003;50:70–73 CrossRef

24. Miwa K, Umeda T, Murata T, et al. **Evaluation of scatter limitation correction: a new method of correcting photopenic artifacts caused by patient motion during whole-body PET/CT imaging.** *Nucl Med Commun* 2016;37:147–54 CrossRef Medline

25. Shidahara M, Watabe H, Kim KM, et al. **Evaluation of a commercial PET tomograph-based system for the quantitative assessment of rCBF, rOEF and rCMRO2 by using sequential administration of 15O-labeled compounds.** *Ann Nucl Med* 2002;16:317–27 CrossRef Medline

26. Hara S, Tanaka Y, Ueda Y, et al. **Noninvasive evaluation of CBF and perfusion delay of Moyamoya disease using arterial spin-labeling MRI with multiple postlabeling delays: comparison with ^{15}O-gas PET and DSC-MRI.** *AJNR Am J Neuroradiol* 2017;38:696–702 CrossRef Medline

27. Kimura H, Kado H, Koshimoto Y, et al. **Multislice continuous arterial spin-labeled perfusion MRI in patients with chronic occlusive cerebrovascular disease: a correlative study with CO2 PET validation.** *J Magn Reson Imaging* 2005;22:189–98 CrossRef Medline

28. Grandin CB, Bol A, Smith AM, et al. **Absolute CBF and CBV measurements by MRI bolus tracking before and after acetazolamide challenge: repeatabilily and comparison with PET in humans.** *Neuroimage* 2005;26:525–35 CrossRef Medline

29. Takasawa M, Jones PS, Guadagno JV, et al. **How reliable is perfusion MR in acute stroke? Validation and determination of the penumbra threshold against quantitative PET.** *Stroke* 2008;39:870–77 CrossRef Medline

30. Sakoh M, Rohl L, Gyldensted C, et al. **Cerebral blood flow and blood volume measured by magnetic resonance imaging bolus tracking after acute stroke in pigs: comparison with [(15)O]H(2)O positron emission tomography.** *Stroke* 2000;31:1958–64 CrossRef Medline

31. Nariai T, Matsushima Y, Imae S, et al. **Severe haemodynamic stress in selected subtypes of patients with Moyamoya disease: a positron emission tomography study.** *J Neurol Neurosurg Psychiatry* 2005; 76:663–69 CrossRef Medline

32. Hirai S, Inaji M, Tanaka Y, et al. **Correlation between clinical presentations and hemodynamic parameters measured by dynamic susceptibility contrast magnetic resonance imaging in adult patients with Moyamoya disease.** *J Stroke Cerebrovasc Dis* 2017; 26:2814–20 CrossRef Medline

33. Ishii Y, Nariai T, Tanaka Y, et al. **Practical clinical use of dynamic susceptibility contrast magnetic resonance imaging for the surgical treatment of Moyamoya disease.** *Neurosurgery* 2014;74:302–09 CrossRef Medline

34. Ishii Y, Tanaka Y, Momose T, et al. **Chronologic evaluation of cerebral hemodynamics by dynamic susceptibility contrast magnetic resonance imaging after indirect bypass surgery for Moyamoya disease.** *World Neurosurg* 2017;108:427–35 CrossRef Medline